Electronic Transactions on Numerical Analysis.
Volume 51, pp. 547–569, 2019.

ISSN 1068–9613.
DOI: 10.1553/etna_vol51s547

ETNA
Kent State University and
Johann Radon Institute (RICAM)

LAMINAR-TURBULENT TRANSITION IN CHANNEL FLOW: WALL EFFECTS AND CRITICAL REYNOLDS NUMBER*

HIDESADA KANDA†

Abstract. This article describes a possible cause of natural laminar-turbulent transition in channel flow, and the minimum critical Reynolds number $R_{c,min}$ is determined. It is assumed that the mechanism of transition is the same for both circular pipe flow and channel flow since each flow has its own minimum critical Reynolds number. Our starting points are that under natural disturbance conditions, transition appears to take place only in the developing entrance region and that the critical Reynolds number R_c becomes $R_{c,min}$ when using a sharp-edged uniform channel. In our previous studies of circular pipe flow, we have developed a model for transition and obtained $R_{c,min} = 1910$ and 1950 in two mesh systems. In this study, for channel flow, the above transition model is verified by obtaining $R_{c,min} = 1190$ and 1260 in two mesh systems.

Key words. hydrodynamic stability, mesh refinement, thermodynamics

AMS subject classifications. 76E05, 65M50, 80A05

1. Introduction.

The notation used in this paper is collected in Appendix A.

1.1. Reynolds' problem.

The laminar-turbulent (L-T) transition in circular pipe flow is one of the fundamental problems of fluid dynamics. Osborne Reynolds in 1883 [22] first found the Reynolds number Re = DV_m/ν and also determined two critical values: an upper critical Reynolds number $R_c \approx 12,800$ by the color-band method and a lower critical Reynolds number $R_{c,min} \approx 2050$, which he called the real critical value, by the pressure-loss method. The precise $R_{c,min}$-value has not yet been agreed upon unanimously. A major unsolved problem is to theoretically obtain the minimum critical Reynolds number $R_{c,min}$. This challenge is called "Reynolds' problem." Why is it difficult to solve Reynolds' problem? It is unclear what causes all the transitions in pipe flow and in channel flow. We suppose that there are two key parameters to the problem:

(i) Regarding the primary parameter of transition, White [32] states that "Transition depends upon many effects, e.g., wall roughness or fluctuations in the inlet stream, but the primary parameter is the Reynolds number." Why is the Reynolds number itself the primary parameter determining L-T transition?

(ii) Regarding the transition length, Reynolds [22] states that "Under no circumstances would the disturbance occur nearer to the trumpet than about 30 diameters in any of the pipes, and the flashes generally but not always commenced at about this distance." Why is the transition point nearer to the pipe or channel inlet, not the inlet itself?

In our previous studies we obtained $R_{c,min} = 2050$ and 2200 experimentally [13] and 1910 and 1950 theoretically [12] based on several assumptions (see Section 1.3). In this study, for channel flow, the above transition model is verified.

1.2. Prerequisites for transition.

(i) The fluid is an incompressible, isothermal, Newtonian fluid with constant viscosity and density, disregarding gravity, external forces, and artificial disturbances. The Reynolds number Re = HV_m/ν ranges from about 500 to about $15,000$.

(ii) The value of R_c depends greatly upon the experimental setup such as the use of calming chamber, baffles, honeycomb, and screens. Accordingly, it is desirable for the initial

*Received August 26, 2019. Accepted November 31, 2019. Published online on December 16, 2019. Recommended by Frank Stenger.

†Department of Computer Science and Engineering, University of Aizu, Aizu-Wakamatsu, Fukushima 965-8580, Japan (hidesada.kanda@gmail.com).

ETNA
Kent State University and
Johann Radon Institute (RICAM)

analysis to avoid geometrically complex channel entrances. Entrance shapes are limited to a sharp-edged inlet and depth-contraction rounded entrances, excluding width-contraction entrances. Channels have smooth-surface walls.

(iii) Each experimental apparatus has two types of R_c-numbers: R_{c1}, R_{c2} from laminar flow to turbulence, and R_{c3} from turbulence to laminar flow (reverse transition). R_{c1} is qualitatively associated with small-magnitude-disturbance conditions at the inlet, and R_{c2} is for medium-magnitude-disturbance conditions.

(iv) The type of disturbances should be natural and not artificial; there is no artificial disturbance generator in a test region or in the fully developed Poiseuille region. A disturbed inlet flow as seen in Reynolds' pressure-loss experiments or a disturbance generator set in front of the inlet is available.

1.3. Assumptions and objectives. Our assumptions are as follows:

(i) The fundamental characteristics of L-T transition are the critical Reynolds number R_c under which no turbulence exists and the transition length x_t, which is defined as the distance from the inlet to the point at which L-to-T transition takes place.

(ii) The mechanism of L-T transition in pipe flow and channel flow (flow between parallel plates) seems to be the same, i.e., both circular pipe flow and channel flow are internal flows bounded by smooth walls and have their own minimum critical Reynolds number $R_{c,min}$ and pressure drops $(\Delta p)_{wc}$ normal to the wall near the inlet (see Figures 5.1 and 5.2). On the contrary, flow on flat plate (boundary-layer flow) is an external flow and does not have its own $R_{c,min}$. However, x_t is one of the key characteristics of L-to-T transition in pipe flow, channel flow, and boundary-layer flow (Section 2.2).

(iii) Consider the transition point. Natural transition to turbulence seems to occur only in the developing entrance region, particularly in the vicinity of the inlet, but does not occur at the inlet itself. No transition appears to occur experimentally in the fully developed Poiseuille region under natural disturbances (see Table 1.1).

Many researchers have concluded that the flow may become turbulent long before it becomes fully developed Poiseuille flow [7, 11, 12]. Taneda [29] claimed that transition in pipe flow occurs only in the entrance region. Badri Narayanan [1] states that in channel flow the spots are born in some region near the entry section and, after traveling some distance, merge. He also states that the transition point lies at $X_t\ (= x_t/(H\mathrm{Re})) = 87/3460 = 0.0251$ for $x_t/H = 87$ and $\mathrm{Re} = 3460$ and that it moves toward upstream, nearer to the entry as Re is increased, and is at $X_t = 12/3850 = 0.00312$ for $x_t/H = 12$ and Re$= 3850$.

(iv) So far, three major aspects have been studied regarding phenomena in the entrance region [6]: (a) a pressure difference between any two sections in the axial direction; (b) a velocity distribution at any section; and (c) the length of the entrance region L_e. According to many previous investigations, variables such as velocity and pressure distributions become similar and independent of the Reynolds number when they are plotted against the dimensionless distance $X\ (= x/(H\mathrm{Re}))$.

(v) Therefore, it is important to find variables which vary in the entrance region, particularly near the pipe or channel inlet. For this purpose, we found the transverse pressure drop $(\Delta p)_{wc}$ between the pressure on the wall and on the centerline (see equation (2.1) [10]); the values of $(\Delta p)_{wc}$ decrease as Re increases, appearing only near the inlet and disappearing downstream as seen in Figure 5.1.

It is noted that $(\Delta p)_{wc}$ cannot be disregarded in the developing entrance region, whereas the boundary-layer approximations disregard this transverse pressure drop.

(vi) From previous experimental results (see Table 1.1), it appears that the value of R_c is determined greatly by the depth-contraction ratio of the entrance sections in two dimensions, not by the width-contraction ratio, i.e., each experimental apparatus has its own R_c and x_t [13].

ETNA
Kent State University and
Johann Radon Institute (RICAM)

TABLE 1.1
Experimental data on the critical Reynolds number and the transition Reynolds number, where A-, D-, and W-, stand for Area-, Depth-, and Width-Contraction, respectively.

Author	D-Con. ratio	Depth H [cm]	Width B [H]	R_c type	R_c or R_t	x_t [x/H]	X_t [x/(H Re)]
Badri Narayanan et al. [1]	W-4	0.318	12	Rc1	3000	?	?
"	"	"	"	Rt	3460	87	0.0251
"	"	"	"	"	3850	12	0.00312
Badri Narayanan [2]	1	1.27	18	Rc3	2800	< 120	< 0.0429
Carlson, Widnall et al. [4]	100	0.6	133	Rc2	1330	?	?
"	"	"	"	Rc3	1120	< 260	< 0.232
Davies, White [5]	1	0.0154	165	Rc2	1440	< 81	< 0.0564
"	"	0.0205	124		"	< 61	< 0.0423
"	"	0.0212	120	"	"	< 59	< 0.0409
"	"	0.0236	108	"	"	< 53	< 0.0368
"	"	0.0244	104	"	"	< 51	< 0.0356
Hartnett, Koh et al. [8]	1	0.791	10	Rc1	1380	?	?
"	"	"	"	Rt	2200	< 36	< 0.0164
"	?	"	"	Rc1	2420	?	?
Karnitz, Potter et al. [14]	24	1.27	70	Rc1	6700	144	0.0215
"	"	"	"	Rt	10000	120	0.0120
Lemoult, Aider et al. [17]	?	2	7.5	Rc1	7330	< 110	< 0.0150
"	"	"	"	Rc3	3770	40	0.0106
Nishioka, Iida et al. [19]	27.4	1.46	27.4	Rc1	10670	< 411	< 0.0385
Patel, Head [21]	1	0.635	48	Rc1	1350	< 203.5	< 0.151
Sano, Tamai [25]	A-20	0.5	180	Rc3	1110	< 640	< 0.578
Seki, Matsubara [26]	34	0.5	52	Rc3	1400	< 100	< 0.0714
Whan, Rothfus [30]	?	1.78	20	Rc2	1420	< 291	< 0.205

In the case of a sharp-edged inlet, R_c takes a minimum critical Reynolds number $R_{c,min}$.

(vii) Possible primary causes of L-T transition are the wall effects based upon Panton's wall model [20] (see Section 3). Lindgren states that "the experiments indicate that real turbulence—both in flashes and in continuous turbulent regions—is maintained by direct action of the bounding walls [18]."

Therefore, the objectives of the present study are as follows:

(1) to confirm the wall effects in determining R_c,

(2) to confirm why the Reynolds number is the primary parameter for L-T transition,

(3) to theoretically obtain $R_{c,min}$ in channel flow, and

(4) to confirm that the above mentioned assumptions apply for determining $R_{c,min}$ in both pipe and channel flows.

2. Characteristics of the entrance flow.

2.1. The entrance length. The entrance region considered in this study includes streamlined contraction, or depth-contraction, entrances. Thus, the inlet ($x = 0$) is the channel inlet for a sharp-edged entrance channel and is the inlet end of the contraction section for contraction entrance channels.

The entrance length x_e is defined as the distance from the inlet to the point downstream where the centerline velocity u_c reaches 99% of its fully developed value ($u_c/V_m = 0.99 \times 1.5 = 1.485$; see (4.8)). Then, for channel flow, the dimensionless entrance length L_e is given for Re ≥ 500 [3, 27] by

$$L_e = \frac{x_e}{H\ \mathrm{Re}} = \frac{0.63}{\mathrm{Re}(0.035\ \mathrm{Re} + 1)} + 0.044 \approx 0.044.$$

ETNA
Kent State University and
Johann Radon Institute (RICAM)

TABLE 2.1
Comparison of length Reynolds number Rx in pipe, channel, and boundary-layer flows.

Author	Flow	Re	x_t/D x_t/H	Rx_t
Reynolds [22]	Bellmouth Pipe	12800	30	3.84×10^5
Rivas, Shapiro [23]	"	–	–	$8 \times 10^4 \sim 4 \times 10^6$
"	"	–	–	5×10^5
Badri Narayanan et al. [1]	W-contract. Chan	3460	87	3.01×10^5
"	"	3850	12	4.62×10^4
Karnitz, Potter, Smith [14]	D-contract. Chan	6700	144	9.65×10^5
"	"	10000	120	1.2×10^6
White [32]	Boundary-layer	–	–	$5 \times 10^5 \sim 3 \times 10^6$

Since the streamlined length in contraction sections is small compared with L_e, the value $L_e \approx 0.044$ can be used both for sharp-edged channels and for contraction-entry channels in this study.

2.2. The transition length. (i) The dimensionless transition length X_t is defined as the normalized distance from the inlet to the transition point as shown in Table 1.1:

$$X_t = \frac{x_t}{H\,\mathrm{Re}}.$$

(ii) Let us compare the transition length of pipe flows, channel flows, and boundary-layer (B-L) flows. For flat-plate boundary-layer flow, the length Reynolds number Rx is used:

$$Rx \equiv \frac{xV_m}{\nu}.$$

Let Rx_t be the length Reynolds number of transition. The relation between Rx_t and the transition length x_t in a pipe and channel flow is expressed as

$$Rx_t = \frac{x_t}{D}\mathrm{Re} \quad \text{(Pipe flow)} \qquad \text{and} \qquad Rx_t = \frac{x_t}{H}\mathrm{Re} \quad \text{(Channel flow)}.$$

For pipe flow and channel flow, in a stream of moderate initial disturbance (i.e., bellmouth or contraction entrance condition), the length Reynolds number of transition Rx_t is of the order of 5×10^5 as seen in Table 2.1. Regarding the flat-plate boundary layer flow, with care in polishing the wall and keeping the free stream quiet, the transition Reynolds number Rx_t is about 3×10^6. However, for typical commercial surfaces and gusty streams, a more realistic value is $Rx_t \approx 5 \times 10^5$ [32]. Thus the value of the length Reynolds number of transition Rx_t is almost the same in pipe, channel, and boundary-layer flows.

Therefore, it is clear that the transition length x_t is one of the fundamental characteristics of L-T transitions together with the critical Reynolds number R_c (see Section 1.3).

2.3. The pressure drop in the entrance region. Here the pressure difference and the pressure drop are defined and distinguished to avoid confusing them. Let the pressure at the inlet be zero (see $x = 0, i = 1$, Figure 3.1).

(i) The axial pressure difference $(\Delta p)_x$ is negative, defined as

$$(\Delta p)_x \equiv p(x + \Delta x) - p(x) = p_{i+1} - p_i < 0$$

and can be used in finite difference expressions, i.e.,

$$\frac{\partial p}{\partial x} \approx \frac{(\Delta p)_x}{\Delta x} < 0.$$

ETNA
Kent State University and
Johann Radon Institute (RICAM)

(ii) The streamwise pressure drop is positive and usually defined as

$$\Delta\mathcal{P}(x) = p(0) - p(x) = 0 - p(x) = -p(x) > 0.$$

(iii) There is the transverse pressure drop $(\Delta p)_{wc}$ in the transverse or normal direction between the pressure on the wall ($p_w = p|_{y=h}$) and on the centerline ($p_c = p|_{y=0}$) (see Section 5.3):

$$(\Delta p)_{wc} = p_w - p_c < 0. \tag{2.1}$$

(iv) The total pressure drop $\Delta\mathcal{P}$ from the channel inlet consists of two components: (a) the pressure drop based on the fully developed flow, $f \cdot (x/H)$, and (b) the excess pressure drop $K(x)$. $K(x)$ is due to the momentum change of the increase in the kinetic energy flux, ΔKE flux(x), and the accumulated increment in the wall shear $K_{\text{Shear}}(x)$ between developing flow and Poiseuille flow [3, 27], i.e.,

$$K(x) = \Delta\text{KE flux}(x) + K_{\text{Shear}}(x). \tag{2.2}$$

Accordingly, $\Delta\mathcal{P}$ can be expressed as

$$\Delta\mathcal{P}(x) = \left(f\frac{x}{H} + \Delta\text{KE flux}'(x) + K'_{\text{Shear}}(x)\right)\left(\frac{1}{2}\rho V_m^2\right) > 0, \tag{2.3}$$

where the Darcy-Weisbach friction factor f is $24/\text{Re}$ for fully developed Poiseuille flow (see (4.11)) and the primes ($'$) denote dimensionless variables (see (6.1) and (6.5)).

The excess pressure drop $K'(x)$ increases monotonically from 0 at $x = 0$ to a constant value $K'(\infty)$ in the fully developed region, and the dimensionless value of $K(\infty)$ is expressed [3, 27] as

$$K'(\infty) = 0.64 + \frac{19}{\text{Re}}.$$

Note that $K'(\infty)$ includes ΔKE flux$'$ of 19/35 (≈ 0.5429) (see (6.5)), which is the increase in the dimensionless kinetic energy flux from the entrance flow to Poiseuille flow.

3. Wall effects and the control-volume method.

3.1. The wall model.

(i) Panton [20] states about a wall model that "the no-slip condition at the wall means that the particles are not translating; however they are undergoing a rotation. We might imagine that the wall consists of an array of marbles, which are rotating but remain at the same location on the wall."

(ii) Accordingly, there are two regions transversely between the channel wall and the centerline in a channel: the wall region and the flow region. Fluid particles in the wall region do not move or change so that the no-slip boundary condition is due to the fluid particles in the wall region. On the other hand, fluid particles in the flow region move downstream.

(iii) The "marbles" of the above statement can be interpreted as an array of "vorticity" in the wall region so that our wall effects are based upon the viscous terms on the wall of the Navier-Stokes equations.

ETNA
Kent State University and
Johann Radon Institute (RICAM)

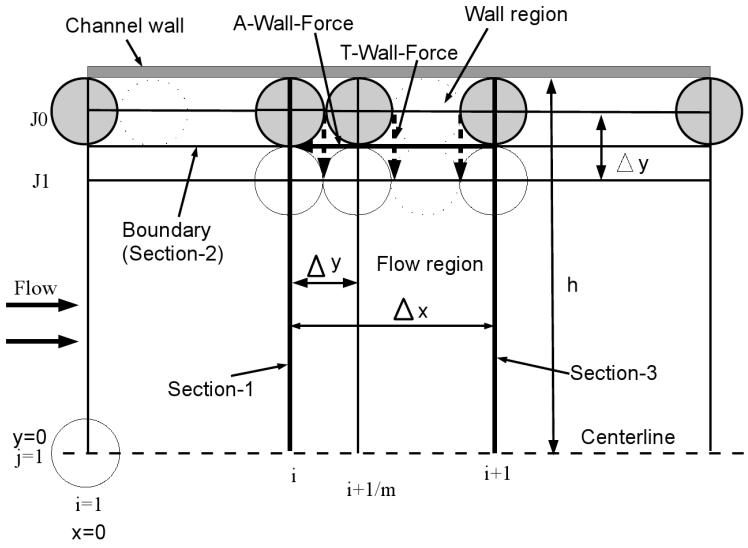

FIG. 3.1. *Axial wall force and transverse wall force in a wall control volume, where the external region (wall region) is inside the channel wall.*

3.2. The wall control-volume system.

(i) Since channel flow is symmetric at the centerline $(y = 0, j = 1)$, here we consider the upper half of the wall and the flow regions in a channel, $[(0 \le y \le h), (1 \le j \le J_0)]$, as displayed in Figure 3.1. Thus, the region for Δx in a channel is enclosed axially by Section-1 $(x = x_i)$ and Section-3 $(x = x_{i+1})$.

(ii) The wall region is the space between the transverse boundary Section-2 $(j = (J_0 + J_1)/2)$ and the wall surface indicated by gray circles of vorticity on the wall $(j = J_0)$.

(iii) The combination of the wall region and the flow region may be called the "wall control volume" since it is similar to that of the "control volume" as shown in Figure 3.2.

Hence there is a difference in the external region: for the wall control volume, the external region is the wall region inside of the channel, whereas for the control volume the external region is outside of the channel. However, we assume that the two external regions similarly exert body forces as the body forces due to external regions are those which act upon the entire flow region or the entire control-volume region.

3.3. Control volume and state function. We refer to the "control-volume method" [31, 32] and thermodynamics [15] to analyze the transverse pressure drop $(\Delta p)_{wc}$ in the wall control volume.

(i) The control-volume method is using a finite region, making a balance of the flow in versus the flow out, and determining gross flow effects such as the force or torque on a body or the total energy exchange.

(ii) In the control volume, body forces are due to external fields (gravity, magnetism, electric potential) which act upon the entire mass within the element; similarly, body forces are due to the wall fields (curl of vorticity, etc.) which act upon the entire fluid in the flow region.

ETNA
Kent State University and
Johann Radon Institute (RICAM)

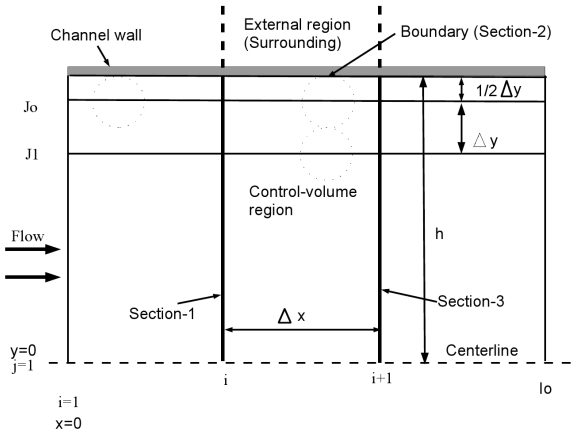

FIG. 3.2. *Control-volume regions, where the external region is outside the channel wall.*

(iii) The concept of the control-volume method is nearly the same as that of the thermodynamic approach.

In thermodynamics, the state of a system is specified in terms of macroscopic state variables such as volume $\mathcal{V}$, pressure p, and temperature T. Functions of state variables such as internal energy U_{int} and enthalpy H are called state functions. Then the enthalpy is defined by

$$H \equiv U_{int} + p\mathcal{V}, \qquad \text{Unit} = [\text{kg m}^2/\text{s}^2], \tag{3.1}$$

where the dimension of $p\mathcal{V}$ is [energy or work; joule] from (3.1).

(iv) For most solids and liquids, at a constant temperature, the energy U_{int} does not change much with pressure ($\Delta U_{int} \approx 0$). Since the change in volume is rather small unless the changes in pressure are very large, the change in enthalpy ΔH due to a change in pressure Δp can be approximated by

$$\Delta H = \Delta(p\mathcal{V}) = p\Delta\mathcal{V} + \mathcal{V}\Delta p \approx \mathcal{V}\Delta p.$$

If the external region performs some work ΔW upon the control-volume region, then

$$\Delta H = \Delta W = \mathcal{V}\Delta p. \tag{3.2}$$

Equation (3.2) means that an applied force due to the external region exerts a body force upon the control-volume region, and the body force does some work (ΔW), which equals ($\mathcal{V}\Delta p$) by Newton's Second Law of Motion. Note that this process may apply to the wall control volume.

3.4. Wall effects and the N-S equations.

(i) In the wall control volume, external forces are due to the axial and transverse viscous terms of the Navier-Stokes equations on the wall or in the wall region.

(ii) The Navier-Stokes equation in vector form is expressed as

$$\rho\left(\frac{\partial V}{\partial t} - V \times \omega\right) = -\nabla\left(p + \frac{1}{2}\rho V^2\right) - \mu(\nabla \times \omega), \tag{3.3}$$

ETNA
Kent State University and
Johann Radon Institute (RICAM)

where V is the velocity vector and p is the difference of the actual pressure from the hydrostatic pressure [6].

Since $V = 0$ on the wall, (3.3) reduces to

$$-\mu(\nabla \times \omega)|_{y=h} = (\nabla p)|_{y=h} < 0, \qquad \text{Unit = [kg/(m}^2\ \text{s}^2)]. \tag{3.4}$$

Vorticity and its curl in two dimensions are defined by

$$\omega_z|_{y=h} \equiv \left(\frac{\partial v}{\partial x} - \frac{\partial u}{\partial y}\right)\bigg|_{y=h} = -\left.\frac{\partial u}{\partial y}\right|_{y=h} = -\left.\frac{du}{dy}\right|_{y=h} \tag{3.5}$$

and

$$(\nabla \times \omega) \equiv \begin{vmatrix} i & j & k \\ \partial/\partial x & \partial/\partial y & 0 \\ 0 & 0 & \omega_z \end{vmatrix} = \frac{\partial \omega_z}{\partial y} i - \frac{\partial \omega_z}{\partial x} j, \tag{3.6}$$

where ω_x and ω_y are zero. Thus the axial and transverse components of the curl of the vorticity in two dimensions are expressed by its definition and (3.4) as

$$\text{Axial:} \quad -\mu(\nabla \times \omega)_x|_{y=h} = -\mu \left.\frac{\partial \omega_z}{\partial y}\right|_{y=h} = \left.\frac{\partial p}{\partial x}\right|_{y=h} < 0, \tag{3.7}$$

$$\text{Transverse:} \quad -\mu(\nabla \times \omega)_y|_{y=h} = \mu \left.\frac{\partial \omega_z}{\partial x}\right|_{y=h} = \left.\frac{\partial p}{\partial y}\right|_{y=h} < 0. \tag{3.8}$$

Therefore the wall effects are based on the axial and transverse viscous terms of the Navier-Stokes equations, respectively.

(iii) We consider body forces due to the upper and lower wall regions. Each term in (3.4) is assumed to be a constant since they are in the fixed wall region.

The volume of the flow region $\mathcal{V}$ is expressed for an axial distance Δx in the channel as $\mathcal{V} = 2b(h - \Delta y)(\Delta x) \approx 2bh(\Delta x)$, where b is the channel width and $H = 2h$ is the channel height or depth. By the integrals of the left term in (3.4), we have

$$\begin{aligned} 2\int_0^b \int_0^h \int_0^{\Delta x} -[\mu(\nabla \times \omega)]_{y=h}\, dx\, dy\, dz &= -2bh(\Delta x)[\mu(\nabla \times \omega)]_{y=h} \\ &= -\mathcal{V}[\mu(\nabla \times \omega)]_{y=h}. \end{aligned}$$

Thus, by multiplying (3.7) and (3.8) by the volume of the flow region $\mathcal{V}$, the applied forces due to the wall control volume or the external forces are expressed as

$$\text{A-Wall-Force} = -\mathcal{V}\,[\mu(\nabla \times \omega)_x]_{y=h}\,, \qquad \text{Units = [kg m/s}^2\text{]}, \tag{3.9}$$

$$\text{T-Wall-Force} = -\mathcal{V}[\mu(\nabla \times \omega)_y]_{y=h}, \tag{3.10}$$

where (A) and (T) denote axial and transverse, respectively. Hereafter, ω denotes ω_z since ω_x and ω_y vanish in two dimensions.

3.5. The vorticity and its curl on the wall. We consider the relation between vorticity and its curl on the wall in the developing entrance region, (3.5) and (3.6). The axial velocity distribution near the wall can be approximated by a quadratic equation or parabola near the wall and a constant in the central part as indicated in Figure 3.3 [28]:

$$u(y) = C\left[1 - \left(\frac{y}{h}\right)^2\right], \tag{3.11}$$

ETNA
Kent State University and
Johann Radon Institute (RICAM)

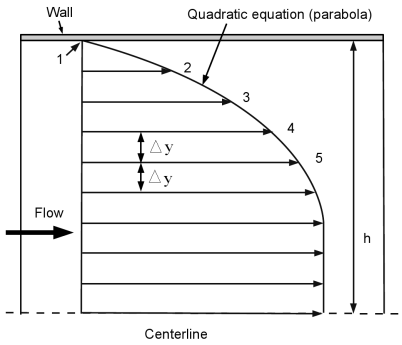

FIG. 3.3. *Axial velocity distribution in the entrance region, where the number indicates transverse mesh points:* $1 = J_0, 2 = J_1, \ldots, 5 = J_4$, *(see Section 8).*

where C is a constant depending on x_i. (For Poiseuille flow, see (4.8)).

Differentiating (3.11) twice with respect to y gives

$$\omega|_{y=h} = -\frac{\partial u}{\partial y}\bigg|_{y=h} = \frac{2C}{h} \qquad \text{and} \qquad \frac{\partial \omega}{\partial y}\bigg|_{y=h} = -\frac{\partial^2 u}{\partial y^2}\bigg|_{y=h} = \frac{2C}{h^2}. \tag{3.12}$$

Accordingly, from (3.7) and (3.12), we have

$$\omega|_{y=h} = h\frac{\partial \omega}{\partial y}\bigg|_{y=h} = h(\nabla \times \omega)_x|_{y=h}. \tag{3.13}$$

4. The axial force and power. In this section, we consider axial forces and powers in both the developing entrance region and the Poiseuille region.

4.1. The wall shear stress and wall effects.

(i) The wall shear stress τ_w is an example of wall effects expressed via (3.12) and (3.13) as

$$\tau_w \equiv \mu\frac{du}{dy}\bigg|_{y=h} = -\mu\,\omega|_{y=h} = -h\left(\mu\frac{\partial \omega}{\partial y}\right)\bigg|_{y=h} = -h[\mu(\nabla \times \omega)_x]_{y=h} < 0. \tag{4.1}$$

(ii) The applied forces due to the wall shear stress τ_w and the axial pressure difference $(\Delta p)_x$ for the small axial distance Δx are related as

$$2b(\Delta x)\tau_w = bH(\Delta p)_x < 0, \qquad \text{Units} = [\text{kg m/s}^2]. \tag{4.2}$$

(iii) From (4.2), we have

$$\tau_w = \frac{h(\Delta p)_x}{\Delta x} = h\frac{\partial p}{\partial x}.$$

4.2. The axial wall and flow forces.

(i) The axial wall force due to the upper and lower wall regions, denoted as A-Wall-Force, is expressed with (3.9) and (4.1) as

$$\begin{aligned} \text{A-Wall-Force} &= -\mathcal{V}\,[\mu(\nabla \times \omega)_x]_{y=h} = -2bh(\Delta x)\,[\mu(\nabla \times \omega)_x]_{y=h} \\ &= 2b(\Delta x)\tau_w < 0. \end{aligned} \tag{4.3}$$

ETNA
Kent State University and
Johann Radon Institute (RICAM)

Similarly, the axial flow force, A-Flow-Force, in the flow region is obtained from the third term of (3.7):

$$\begin{aligned}\text{A-Flow-Force} &= 2\int_0^b\int_0^h\int_0^{\Delta x}\left[\frac{\partial p}{\partial x}\right]_{y=h} dx\,dy\,dz \\ &\approx 2\int_0^b\int_0^h\int_0^{\Delta x}\left[\frac{\partial p}{\partial x}\right] dx\,dy\,dz = 2bh(\Delta p)_x = bH(\Delta p)_x.\end{aligned} \tag{4.4}$$

(ii) By Newton's Second Law, A-Wall-Force exerts an equal force, A-Flow-Force, on the fluid in the flow region: i.e., A-Wall-Force = A-Flow-Force.

Although equation (4.2) is usually derived from the N-S equation, it is also verified by the wall control-volume method from (4.3) and (4.4).

4.3. The axial wall and flow powers. The wall region does not move, but the fluid in the flow region travels relatively downstream with mean velocity V_m. Therefore, A-Wall-Force performs negative work on the fluid in the flow region, resulting in a pressure difference in the axial direction. This negative work can be called the axial wall power (A-Wall-Power), and the energy loss of the fluid is called the axial flow power (A-Flow-Power), and their dimension is that of power, energy/time, as measured in watts (W = J/s, [kg m^2/s^3]).

The axial wall power and axial flow power, denoted as A-Wall-Power and A-Flow-Power, respectively, are derived by multiplying (4.3) and (4.4) by V_m:

$$\begin{aligned}\text{A-Wall-Power} &= -\left\{\mathcal{V}\left[\mu(\nabla\times\omega)_x\right]_{y=h}\right\}V_m = -Q(\Delta x)[\mu(\nabla\times\omega)_x]_{y=h} \\ &= -\left\{2bh(\Delta x)\left[\mu(\nabla\times\omega)_x\right]_{y=h}\right\}V_m = 2b(\Delta x)\tau_w V_m\end{aligned} \tag{4.5}$$

and

$$\text{A-Flow-Power} = 2bh(\Delta p)_x V_m = Q(\Delta p)_x, \tag{4.6}$$

where $Q = 2bhV_m$ is the volumetric flux. A-Wall-Power is made dimensionless by dividing (4.5) by $Q[(1/2)\rho V_m^2]$:

$$\text{A-Wall-Power}' = -\frac{Q(\Delta x)\left[\mu(\nabla\times\omega)_x\right]_{y=h}}{Q[(1/2)\rho V_m^2]} = -\frac{(\Delta x)\left[\mu(\nabla\times\omega)_x\right]_{y=h}}{[(1/2)\rho V_m^2]}. \tag{4.7}$$

Similarly, dividing (4.6) by $Q[(1/2)\rho V_m^2]$ yields

$$\text{A-Flow-Power}' = \frac{Q(\Delta p)_x}{Q[(1/2)\rho V_m^2]} = (\Delta p')_x.$$

4.4. The dimensionless A-Wall-Power in Poiseuille flow. In Poiseuille flow, the axial velocity distribution u is obtained by replacing C in (3.11) with $(3/2)V_m$:

$$u(y) = \frac{3}{2}V_m\left[1-\left(\frac{y}{h}\right)^2\right]. \tag{4.8}$$

Differentiating (4.8) twice with respect to y gives

$$\omega|_{y=h} = -\left.\frac{\partial u}{\partial y}\right|_{y=h} = \frac{3V_m}{h} \qquad \text{and} \qquad \left.\frac{\partial \omega}{\partial y}\right|_{y=h} = -\left.\frac{\partial^2 u}{\partial y^2}\right|_{y=h} = \frac{3V_m}{h^2}. \tag{4.9}$$

ETNA
Kent State University and
Johann Radon Institute (RICAM)

Accordingly, from (3.7) and (4.9), we have

$$\omega|_{y=h} = h\frac{\partial \omega}{\partial y}\bigg|_{y=h} = h(\nabla \times \omega)_x|_{y=h}. \tag{4.10}$$

It is noted that equations (3.13) and (4.10) are the same, satisfied in both the developing entrance region and the Poiseuille region.

From (4.7), (4.9), and (4.10), we have

$$\text{A-Wall-Power}' = -\frac{(\Delta x)[(3\mu V_m)/h^2]}{[(1/2)\rho V_m^2]} = -\frac{24}{\text{Re}}\frac{\Delta x}{H} = -24\Delta X, \tag{4.11}$$

where ($f = 24/\text{Re}$) is the Darcy-Weisbach friction factor for Poiseuille flow (see (2.3)).

5. The transverse force and power. We consider transverse forces and powers in the developing entrance region. Note that they are zero in the Poiseuille region.

5.1. The transverse wall and flow forces.

(i) The transverse wall force (T-Wall-Force) in the upper and lower wall regions is similarly written by (3.8) and (3.10) as

$$\begin{aligned} \text{T-Wall-Force} &= -\mathcal{V}[\mu(\nabla \times \omega)_y]_{y=h} = -2bh(\Delta x)[\mu(\nabla \times \omega)_y]_{y=h} \\ &= 2bh(\Delta x)\left[\mu(\frac{\partial \omega}{\partial x})\right]_{y=h} = 2bh(\mu \Delta \omega)_x|_{y=h} < 0. \end{aligned} \tag{5.1}$$

(ii) T-Wall-Force exerts an equal transverse flow force (T-Flow-Force) on the fluid in the flow region in the transverse direction, resulting in a transverse pressure drop $(\Delta p)_{wc}$ as indicated in Figure 5.1. Then T-Flow-Force for Δx is given by

$$\begin{aligned} \text{T-Flow-Force} &= 2\int_0^b \int_0^h \int_0^{\Delta x} \left[\frac{\partial p}{\partial y}\right]_{y=h} dx\, dy\, dz \\ &\approx 2b(\Delta x)\int_0^h \left[\frac{\partial p}{\partial y}\right] dy \approx 2b(\Delta x)(\Delta p)_y = 2b(\Delta x)(\Delta p)_{wc} < 0, \end{aligned} \tag{5.2}$$

where T-Flow-Force = T-Wall-Force by Newton's Second Law.

It is noted from Figure 5.1 that $(\Delta p)_{wc}$ defined in (2.1) decreases as Re increases and appears only near the inlet and disappears downstream, which are variable conditions for determining L-to-T transition in channel flow.

(iii) For pipe flow, we similarly have obtained the pressure drop in the radial direction (see Figure 5.2, copied from [9]). From Figures 5.1 and 5.2, the L-to-T transition process appears to be the same in both pipe and channel flows.

5.2. T-Wall-Force, acceleration of fluid, and L-to-T transition. We consider the relation between T-Wall-Force and R_c.

(i) T-Wall-Force and $(\Delta p)_{wc}$ satisfy the conditions for variables that vary in the entrance region, particularly near the channel inlet (see Section 1.3).

In the previous study, from $(\Delta p)_{wc}$, we have obtained $R_{c,\min} \approx 910$ when using (b) $J_0 = 51$ mesh points in the transverse direction and $R_{c,\min} \approx 1230$ when (c) $J_0 = 101$ for channel flow (see Table 7.2) [10].

(ii) In this study, we try to obtain new values of $R_{c,\min}$ from T-Wall-Force and to verify the method since T-Wall-Force is the primary cause and T-Flow-Force or $(\Delta p)_{wc}$ is the secondary result.

ETNA
Kent State University and
Johann Radon Institute (RICAM)

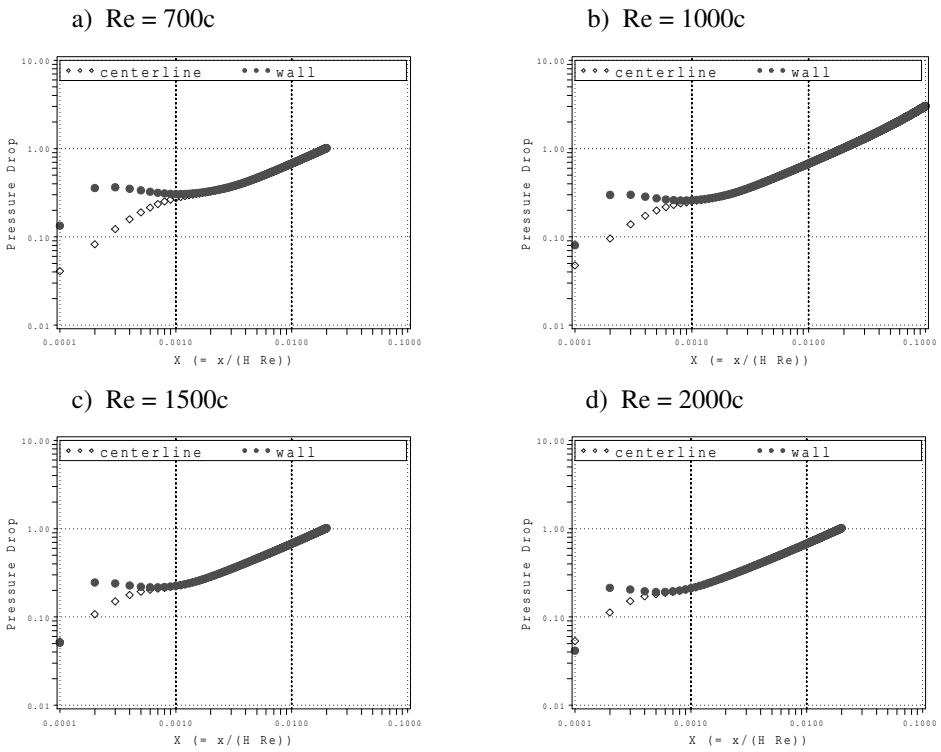

FIG. 5.1. *Channel flow: Axial pressure drop with* $(\Delta p)_{wc}$ *due to |T-Flow-Force|, where the mesh system is (c)* $J_0 = 101$ *(see Section 7.2). From Kanda [10].*

(iii) Accordingly, from (3.3), (5.1), and (5.2), it is possible to assume the following process for the acceleration of the fluid to Poiseuille flow in the flow region:

(a) T-Wall-Force in the wall region exerts an equal transverse force T-Flow-Force on the fluid in the flow region by Newton's Second Law.

(b) T-Wall-Force and T-Flow-Force cause the fluid in the flow region to move towards the centerline in the transverse direction as shown in Figure 3.1, resulting in an increase in kinetic energy.

(c) An increase in kinetic energy means that the pressure of the fluid decreases as can be seen in the first term on the right-hand side of (3.3). T-Flow-Force shows a result of this change.

(d) T-Flow-Force shows that the pressure on the centerline is higher than that on the wall. As explained in (b) above, however, the fluid near the centerline does not move towards the wall.

(e) Thus T-Wall-Force and T-Flow-Force work as acceleration forces together with the "equation of continuity."

(f) Hence, the onset of L-to-T transition should depend on whether or not the acceleration power provided by T-Wall-Force exceeds a required value of ΔKE flux.

5.3. The transverse flow work and flow power. We consider T-Flow-Work (transverse flow work) done on the fluid by T-Wall-Force.

(i) T-Wall-Force yields transverse velocity v and pressure drop $(\Delta p)_{wc}$ in the transverse direction.

ETNA
Kent State University and
Johann Radon Institute (RICAM)

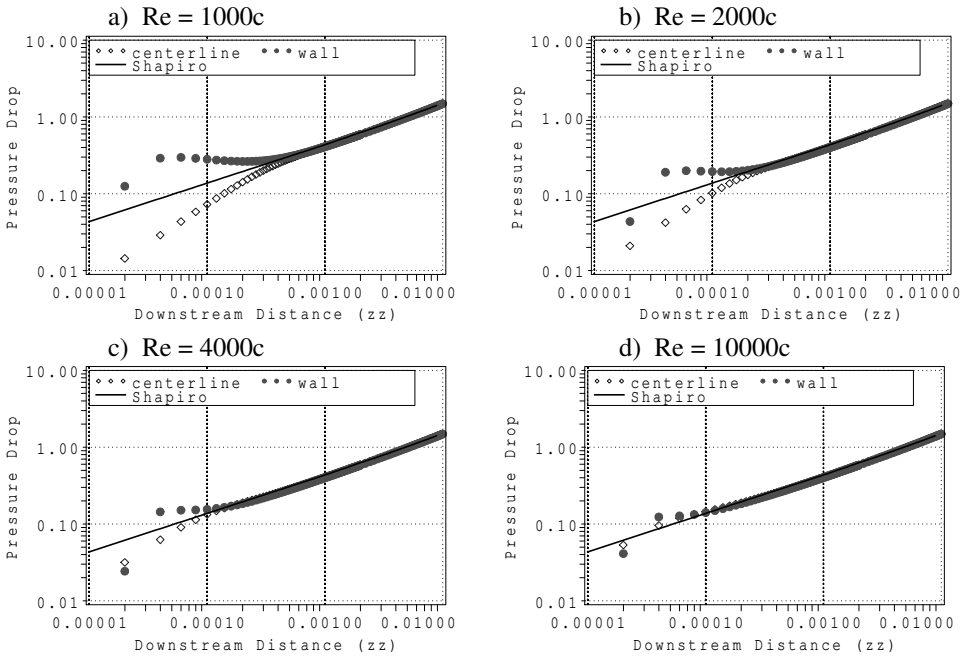

FIG. 5.2. *Pipe flow: Axial pressure drop with* $(\Delta p)_{wc}$ *due to |R-Flow-Force|, (Radial-Flow-Force), where the downstream distance (zz) =* X *and the mesh system is (c)* $J_0 = 101$. *From Kanda [9].*

(ii) Equation (3.2) can be applied to incompressible flow as well so that T-Flow-Work is expressed as

$$\text{T-Flow-Work} = \mathcal{V}(\Delta p)_{wc} = 2bh(\Delta x)(\Delta p)_{wc}. \tag{5.3}$$

Note that the dimension of $\mathcal{V}(\Delta p)_{wc}$ is physically equivalent to energy, and by multiplying by a frequency (inverse of a period, $\omega|_{y=h}$), the unit of $[\mathcal{V}(\Delta p)_{wc}(\omega|_{y=h})]$ becomes that of power (see (5.8)).

(iii) The pressure drop in the transverse direction is approximated by the mean difference in the pressure between x_i and x_{i+1},

$$(\Delta p_i)_{wc} \approx \frac{1}{2}[(p_{i,J_0} + p_{i+1,J_0}) - (p_{i,1} + p_{i+1,1})]. \tag{5.4}$$

(iv) The period during which T-Wall-Force acts on the flow passing along vorticity ω_{i,J_0} and vorticity ω_{i+1,J_0} on the wall is considered. The period Δt_i^* may be estimated by dividing the axial mesh space Δx by the mean velocity at two points (i, J_1) and $(i+1, J_1)$.

$$\Delta t_i^* = \frac{\Delta x}{(1/2)(u_{i,J_1} + u_{i+1,J_1})} \approx \frac{\Delta x}{u_{i+1/2,J_1}}.$$

However, if this Δt_i^* is the correct period, then an inconsistency is encountered. Three simple cases are considered as examples to illustrate this inconsistency.

(a) First, if the mesh aspect ratio is $\Delta x = 2\Delta y$, $(m = 2)$, as indicated in Figure 3.1, where Δx is constant, then T-Flow-Work(a) and T-Flow-Power(a) can be expressed as

$$\text{T-Flow-Work}(a) = \mathcal{V}(\Delta p)_{wc}, \tag{5.5}$$

$$\text{T-Flow-Power}(a) = \frac{\mathcal{V}(\Delta p)_{wc}}{\Delta x/(u_{i+1/2,J1})} = \frac{\mathcal{V}(\Delta p)_{wc}\,(u_{i+1/2,J1})}{2\Delta y}.$$

ETNA
Kent State University and
Johann Radon Institute (RICAM)

(b) Next, if Δx and $\mathcal{V}$ are equally divided into two parts, then $\Delta x = \Delta y + \Delta y$ and $\mathcal{V} = \mathcal{V}1 + \mathcal{V}2$. T-Flow-Work$(b)$ in $\mathcal{V}$ is calculated by adding work in $\mathcal{V}1$ and work in $\mathcal{V}2$:

$$\text{T-Flow-Work}(b) = \mathcal{V}1(\Delta p1)_{wc} + \mathcal{V}2(\Delta p2)_{wc} \approx \mathcal{V}(\Delta p)_{wc}. \tag{5.6}$$

T-Flow-Power(b) in $\mathcal{V}$ is calculated by adding the power in $\mathcal{V}1$ and the power in $\mathcal{V}2$,

$$\begin{aligned}\text{T-Flow-Power}(b) &= \frac{\mathcal{V}1(\Delta p1)_{wc}}{\Delta y/(u_{i+1/4,J_1})} + \frac{\mathcal{V}2(\Delta p2)_{wc}}{\Delta y/(u_{i+3/4,J_1})} \\ &\approx \frac{\mathcal{V}(\Delta p)_{wc}\,(u_{i+1/2,J_1})}{\Delta y} \approx 2\ \text{T-Flow-Power}(a),\end{aligned}$$

where it is assumed that $(\Delta p1)_{wc} \approx (\Delta p2)_{wc} \approx (\Delta p)_{wc}$ and $u_{i+1/4,J_1} \approx u_{i+3/4,J_1} \approx u_{i+1/2,J_1}$. From (5.5) and (5.6), T-Flow-Work(a) equals T-Flow-Work(b). Comparing T-Flow-Power(a) and T-Flow-Power(b), however, T-Flow-Power(b) is twice the value of T-Flow-Power(a) although the volume and position are the same.

(c) In numerical calculations, usually $\Delta x = m\Delta y$ ($m = 1, 2, 3, \dots$). To avoid the inconsistency between T-Flow-Power(a) and T-Flow-Power(b) above, the following period is required for a general mesh system of $\Delta x = m\Delta y$:

$$\Delta t_i = \frac{\Delta y}{(1/2)(u_{i,J_1} + u_{i+1,J_1})} \approx \frac{1}{(1/2)(\omega_{i,J_0} + \omega_{i+1,J_0})} \approx \frac{1}{\omega_{i+1/2,J_0}}. \tag{5.7}$$

This period in (5.7) is based on the following assumptions: Rotation of a fluid particle on the wall yields a vortex and a vorticity. Then the curl of the vorticity yields T-Wall-Force from (5.1). The diameter of vorticities on the wall is Δy. Accordingly, T-Wall-Force is produced between two continuous vortexes or per Δy.

(v) T-Flow-Power is derived from (5.3), (5.4), and (5.7):

$$\text{T-Flow-Power} = [\mathcal{V}(\Delta p_i)_{wc}] \cdot (\omega_{i+1/2,J_0}) = [2bh\Delta x(\Delta p_i)_{wc}] \cdot (\omega_{i+1/2,J_0}). \tag{5.8}$$

5.4. The transverse wall work and wall power.

(i) T-Wall-Work can be expressed by (5.1) as:

$$\begin{aligned}\text{T-Wall-Work} &= (\text{T-Wall-Force}) \times h = -\mathcal{V}h[\mu(\nabla \times \omega)_y]_{y=h} \\ &= -2bh^2(\Delta x)[\mu(\nabla \times \omega)_y]_{y=h} = 2bh^2(\mu\Delta\omega)_x|_{y=h}.\end{aligned}$$

(ii) The transverse wall power (T-Wall-Power) is obtained from (5.7) by multiplying T-Wall-Work by the vorticity $(\omega|_{y=h})$:

$$\text{T-Wall-Power} = (\text{T-Wall-Work}) \cdot \omega = [2bh^2(\mu\Delta\omega)_x|_{y=h}] \cdot (\omega_{i+1/2,J_0}). \tag{5.9}$$

6. A criterion for determining $\mathbf{R_c}$.

6.1. Dimensionless variables. In the numerical calculations, dimensionless variables denoted with prime ($'$) are used:

$$\begin{aligned} x' &= \frac{x}{H}, \quad y' = \frac{y}{H}, \quad \omega' = \frac{\omega}{V_m/H}, \quad p' = \frac{p}{(1/2)\rho V_m^2}, \\ t' &= \frac{V_m}{H}t, \quad \psi' = \frac{\psi}{H^2 V_m}, \quad X = \frac{x}{H\text{Re}}, \end{aligned} \tag{6.1}$$

where t' is the time, ψ' is the stream function, and x' and X are the dimensionless axial coordinates. Note that x' ($= x/H$) is used for the numerical calculation, and X ($= x/(H\ \text{Re})$) is used in the figures and tables.

ETNA
Kent State University and
Johann Radon Institute (RICAM)

6.2. The kinetic energy flux.

(i) Consider the kinetic energy flux (KE flux) at the inlet. KE flux varies with inlet shapes such as rounded contractions and with transverse velocities. In this study, the inlet shape is without any contraction, and the velocity profile is the mean axial velocity V_m only. Then the kinetic energy flux across the inlet, where the channel width is b, is given by

$$\text{KE flux}_{\text{Inlet}} = 2\int_0^h V_m \left(\frac{1}{2}\rho V_m^2\right) b\, dy = 2bhV_m \left(\frac{1}{2}\rho V_m^2\right) = Q\left(\frac{1}{2}\rho V_m^2\right). \tag{6.2}$$

In this case, KE $\text{flux}_{\text{Inlet}}$ has a constant value for channel flow, so we define KE $\text{flux}_{\text{Mean}}$ as

$$\text{KE flux}_{\text{Mean}} \equiv Q\left(\frac{1}{2}\rho V_m^2\right).$$

Note that the unit of KE flux is that of power. In the fully developed Poiseuille flow, the streamwise velocity distribution is given by (4.8), and the kinetic energy flux of channel Poiseuille flow is

$$\text{KE flux}_{\text{Poiseuille}} = 2\int_0^h \left(\frac{1}{2}\rho\right)\left(\frac{3}{2}V_m\left[1-(\frac{y}{h})^2\right]\right)^3 b\, dy = \frac{54}{35}Q\left(\frac{1}{2}\rho V_m^2\right). \tag{6.3}$$

Then, ΔKE flux is expressed as

$$\Delta\text{KE flux} = \text{KE flux}_{\text{Poiseuille}} - \text{KE flux}_{\text{Inlet}}. \tag{6.4}$$

(ii) KE flux and ΔKE flux are made dimensionless by dividing by KE $\text{flux}_{\text{Mean}}$. From (6.2), (6.3), and (6.4), the dimensionless ΔKE flux is given by

$$\Delta\text{KE flux}' = \frac{\Delta\text{KE flux}}{\text{KE flux}_{\text{Mean}}} = \frac{\Delta\text{KE flux}}{Q[(1/2)\rho V_m^2]} = \frac{54}{35} - 1 = \frac{19}{35} \approx 0.5429. \tag{6.5}$$

6.3. The dimensionless T-Wall-Power and T-Flow-Power. Let the total transverse wall power and the total transverse flow power be denoted as T-T-Wall-Power and T-T-Flow-Power, respectively.

(i) For a sharp-edged inlet channel, the dimensionless T-Wall-Power$'$ is reduced from (5.9) and (6.1) to

$$|\text{T-Wall-Power}'| = \left|\frac{2bh^2[(\mu\Delta\omega)_x]\cdot\omega}{Q[(1/2)\rho V_m^2]}\right| = \frac{1}{\text{Re}}\left|(\Delta\omega')_x\cdot\omega'\right|_{y=h}, \tag{6.6}$$

and thus,

$$|\text{T-T-Wall-Power}'| = \frac{1}{\text{Re}}\sum_{i=2}^{I_1}\left|(\Delta\omega')_x\cdot\omega'\right|_{y=h}. \tag{6.7}$$

In the numerical calculation, we have

$$\omega' \approx \frac{1}{2}(\omega_i' + \omega_{i+1}'), \qquad (\Delta\omega')_x = (\omega_{i+1}' - \omega_i'), \qquad \text{and}$$
$$\omega'(\Delta\omega')_x \approx \frac{1}{2}(\omega_i' + \omega_{i+1}')\cdot(\omega_{i+1}' - \omega_i') = \frac{1}{2}(\omega_{i+1}'^2 - \omega_i'^2).$$

ETNA
Kent State University and
Johann Radon Institute (RICAM)

Therefore, equation (6.6) yields

$$|\text{T-Wall-Power}'| \approx \frac{1}{2\text{Re}}|(\omega_{i+1}'^2 - \omega_i'^2)|_{y=h}.$$

Regarding |T-T-Wall-Power′|, we have

$$|\text{T-T-Wall-Power}'| \approx \frac{1}{2\text{Re}}\sum_{i=2}^{I_1}|(\omega_{i+1}'^2 - \omega_i'^2)|_{y=h} = \frac{1}{2\text{Re}}|(\omega_{i=2}'^2 - 6^2)|_{y=h}, \tag{6.8}$$

where if $I_1 (= I_0 - 1)$ indicates the Poiseuille region, then $\omega'|_{y=h} = 6$ from (4.9) and (6.1).

(ii) The dimensionless T-Flow-Power is obtained from (5.8) as

$$|\text{T-Flow-Power}'| = \frac{|2bh(\Delta x)(\Delta p)_{wc} \cdot \omega|}{Q[(1/2)\rho V_m^2]} = |(\Delta x')(\Delta p')_{wc} \cdot \omega'|_{y=h},$$

and thus,

$$|\text{T-T-Flow-Power}'| = \sum_{i=2}^{I_1}|(\Delta x')(\Delta p')_{wc} \cdot \omega'|_{y=h}. \tag{6.9}$$

6.4. Determination of $\mathbf{R_c}$. This section follows Section 5.2.

(i) |T-T-Wall-Power| decreases as Re increases, whereas ΔKE flux is constant. Therefore, the criteria for determining R_c depends upon the relation between |T-T-Wall-Power| and ΔKE flux. Thus, the criteria for determining R_c are

$$|\text{T-T-Wall-Power}| \begin{cases} > \Delta\text{KE flux}, & \text{no transition}, \\ = \Delta\text{KE flux}, & \text{Re} = R_c, \text{ and} \\ < \Delta\text{KE flux}, & \text{a transition occurs}. \end{cases}$$

If $|\text{T-T-Wall-Power}'| = \Delta\text{KE flux}' = (19/35)$, then Re = $R_{c,\min}$ from (6.7) and (6.8):

$$\text{Re} = R_{c,\min} = \frac{35}{19}\sum_{i=2}^{I_1}|(\Delta\omega')_x \cdot \omega'|_{y=h} \approx \frac{35}{38}|(\omega_{i=2}'^2 - 6^2)|_{y=h}. \tag{6.10}$$

However, since |T-T-Wall-Power′| depends upon Re, it is difficult to directly calculate $R_{c,\min}$ from (6.10). Therefore $R_{c,\min}$ is obtained in two steps: (a) |T-T-Wall-Power′| from (6.8) and (b) via linear interpolation as can be seen in Table 7.2 and Figure 7.2.

(ii) It is noted that equations (6.8) and (6.10) show a possible reason why Re is the primary parameter for L-T transition in channel flow [32].

(iii) When |T-T-Wall-Power| > ΔKE flux, the difference between |T-T-Wall-Power| and ΔKE flux might be maintained in the internal energy of the fluid, restoring to the pressure of the fluid.

(iv) Since T-Flow-Power equals T-Wall-Power, the criteria for determining R_c can be written as follows [10]:

$$|\text{T-T-Flow-Power}| \begin{cases} > \Delta\text{KE flux}, & \text{no transition}, \\ = \Delta\text{KE flux}, & \text{Re} = R_c, \text{ and} \\ < \Delta\text{KE flux}, & \text{a transition occurs}. \end{cases} \tag{6.11}$$

Therefore, if $|\text{T-T-Flow-Power}'| = \Delta\text{KE flux}' = (19/35)$, then Re = $R_{c,\min}$ from (6.9) and (6.11).

ETNA
Kent State University and
Johann Radon Institute (RICAM)

6.5. The stability of Poiseuille flow.

(i) We consider the reason why Poiseuille flow is stable by examining the shear stress $\mu(du/dy)$. The shear forces exert on a fluid some shear stresses at y and $(y + \Delta y)$ for Δx, denoted as τ-force$_1$ and τ-force$_2$, respectively. From (4.8), we have

$$\tau\text{-force}_1 = (b\Delta x)\mu\frac{du}{dy} = -\frac{3\mu V_m b(\Delta x)y}{h^2},$$
$$\tau\text{-force}_2 = (b\Delta x)\mu\frac{du}{dy} = -\frac{3\mu V_m b(\Delta x)(y+\Delta y)}{h^2}.$$

Then the shear force per unit volume is expressed by subtracting τ-force$_1$ from τ-force$_2$, resulting in the constant axial pressure difference:

$$\begin{aligned}\frac{\tau\text{-force}_2 - \tau\text{-force}_1}{b\Delta x\Delta y} &= -\frac{3\mu V_m}{h^2} = -\frac{12\mu V_m}{H^2}\frac{(1/2)\rho V_m^2}{(1/2)\rho V_m^2} \\ &= -\frac{24\mu}{\rho H V_m}\frac{1}{H}\left(\frac{1}{2}\rho V_m^2\right) = -\frac{24}{\mathrm{Re}}\frac{1}{H}\left(\frac{1}{2}\rho V_m^2\right) = \frac{(\Delta p)_x}{\Delta x}.\end{aligned} \tag{6.12}$$

From (6.12), the Darcy-Weisbach friction factor $f = 24/\mathrm{Re}$ in (2.3) is obtained. Thus, the constant shear force $(-3\mu V_m/h^2)$ is active across the height or depth in the entire Poiseuille region, so that transition to turbulence will not occur in the Poiseuille region.

(ii) If large artificial disturbances are given in Poiseuille flow, then Poiseuille flow changes to a disturbed turbulent flow. Regarding pipe flow, Leite states [16] that "The small disturbances introduced by the periodic motion of the sliding sleeve decayed as they travel downstream for all the Reynolds numbers at which the measurements were taken (i.e., up to Re = 13,000). Larger disturbances introduced by the motion of the ring airfoil did not decay at all Reynolds numbers."

7. Calculation of $\mathbf{R_{c,min}}$. Part of this section refers to previous calculations [10].

7.1. Governing equations. We introduce the stream function and vorticity formulae in two-dimensional Cartesian coordinates as governing equations to avoid the explicit appearance of the pressure term. Accordingly, the velocity fields are determined without any assumptions regarding pressure. Subsequently, the pressure distribution is calculated using values of the velocity fields.

Let ψ be the stream function. The dimensionless transport equation for the vorticity ω is expressed as

$$\frac{\partial\omega}{\partial t} + \frac{\partial\psi}{\partial y}\frac{\partial\omega}{\partial x} - \frac{\partial\psi}{\partial x}\frac{\partial\omega}{\partial y} = \frac{1}{\mathrm{Re}}\nabla^2\omega.$$

The Poisson equation for the stream function is given by

$$\nabla^2\psi = -\omega.$$

The axial velocity u and transverse velocity v are defined as derivatives of the stream function,

$$u = \frac{\partial\psi}{\partial y}, \qquad v = -\frac{\partial\psi}{\partial x}. \tag{7.1}$$

The pressure can be calculated from the steady-state form of the Navier-Stokes equations. The pressure distribution for the x-partial derivative is

$$\frac{\partial p}{\partial x} = -2\left(u\frac{\partial u}{\partial x} + v\frac{\partial u}{\partial y}\right) + \frac{2}{\mathrm{Re}}\nabla^2 u \tag{7.2}$$

ETNA
Kent State University and
Johann Radon Institute (RICAM)

and that for the y-partial derivative is

$$\frac{\partial p}{\partial y} = -2\left(u\frac{\partial v}{\partial x} + v\frac{\partial v}{\partial y}\right) + \frac{2}{\mathrm{Re}}\nabla^2 v. \tag{7.3}$$

Since u and v are known at every point from (7.1), a smooth pressure distribution that satisfies both (7.2) and (7.3) is calculated using the Poisson equation for the pressure [24],

$$\nabla^2 p = \frac{\partial^2 p}{\partial x^2} + \frac{\partial^2 p}{\partial y^2} = -4\left[\frac{\partial v}{\partial x}\frac{\partial u}{\partial y} - \frac{\partial u}{\partial x}\frac{\partial v}{\partial y}\right]. \tag{7.4}$$

For the calculation of the pressure distribution, it is important to make no assumptions. Accordingly, the vorticity transport is solved first and then the pressure distribution equations are solved. The initial values are determined using (7.2), and then (7.4) is used to obtain better approximations.

7.2. The numerical method and the mesh system. The finite difference equations for both the stream function-vorticity and the pressure are solved by the Gauss-Seidel iterative method. This computational scheme uses the Forward-Time, Centered-Space (FTCS) method. The scheme has second-order accuracy in the space variables and first-order accuracy in time. The used rectangular mesh system is schematically illustrated in Figure 3.1, where I_0 and J_0 are the maximum coordinates for the axial and transverse mesh points, respectively, and $I_1 = I_0 - 1$ and $J_1 = J_0 - 1$. Here, J_0 means on the wall, and J_1 means at the wall. To calculate T-Wall-Power and T-Flow-Power, two mesh systems (b) and (c) are used, where ΔX = 0.0001, $\Delta x = \mathrm{Re}\Delta X$:

(b) $J_0 = 51$, $I_0 = 1001$, $\max X = 0.1$, and four Reynolds numbers, $1000, 2000, 4000,$ and $10,000$; (c) $J_0 = 101$, for three Re $= 700, 1500,$ and 2000, $I_0 = 201$, $\max X = 0.02$, and for Re $= 1000$, $I_0 = 1001$, and $\max X = 0.1$.

7.3. The vorticity on the wall. For the vorticity, the boundary condition at the no-slip walls is derived from (3.5). Using a three-point, one-sided approximation for derivatives, we obtain

$$\omega_{i,J_0} = -\left.\frac{\partial u}{\partial y}\right|_{y=h} \approx -\frac{3u_{i,J_0} - 4u_{i,J_1} + u_{i,J_2}}{2\triangle y} = \frac{4u_{i,J_1} - u_{i,J_2}}{2\triangle y}. \tag{7.5}$$

The boundary conditions for the axial velocity at the channel inlet ($i = 1$) are approximated as

$$u_{1,j} = 1, \qquad 1 \le j \le J_1, \qquad \text{and} \qquad u_{1,J_0} = 0.$$

Table 7.1 displays the calculated results for the vorticity on the wall, where a large value of vorticity may appear at a channel inlet edge; ω_{1,J_0} at the channel inlet is 150 for $J_0 = 51$ ($\Delta y \approx 0.01$) and 300 for $J_0 = 101$ ($\Delta y \approx 0.005$); if $\Delta y \to 0$, then $\omega_{1,J_0} \to \infty$. In the FTCS method, ω_{1,J_0} is not used so that a reasonable $\omega|_{y=h}$ can be observed in Table 7.1.

7.4. Calculation of $\mathbf{R_{c,min}}$. |T-T-Wall-Power| and |T-T-Flow-Power| are obtained from (6.8) and (6.9), respectively, and the calculated results are displayed in Table 7.2 and Figure 7.1.

From (6.10), if $|\text{T-T-Wall-Power}'| = \Delta\text{KE flux}' = (19/35) = 0.5429$, then Re = $R_{\text{c,min}}$. The minimum critical Reynolds number $R_{\text{c,min}}$ is obtained via linear interpolation as indicated in Figure 7.2.

For (b) $J_0 = 51$, |T-T-Wall-Power|, Re1 $= 1000$, and Re2 $= 2000$,

$$\frac{R_{\text{c,min}} - 1000}{0.5429 - 0.6555} = \frac{2000 - 1000}{0.228 - 0.6555}, \qquad \text{so} \qquad R_{\text{c,min}} = 1260.$$

ETNA
Kent State University and
Johann Radon Institute (RICAM)

TABLE 7.1
Vorticity at ($i = 2, j = J_0$) vs. X and Re, where (b) J_0 = 51 and (c) J_0 = 101.

X / Re	500-b	1000-b	2000-b	4000-b	700-c	1000-c	1500-c	2000-c
0.0001	47.970	36.701	30.793	28.013	41.849	36.790	32.792	30.767
0.0002	23.284	18.917	17.821	18.433	19.945	18.540	17.778	17.675
0.0003	16.760	15.197	15.731	16.803	15.424	15.097	15.310	15.718
0.0005	13.183	13.556	14.655	15.185	13.074	13.520	14.215	14.650
0.0007	12.149	13.095	13.889	14.077	12.465	13.071	13.645	13.883
0.001	11.554	12.542	12.902	12.929	12.034	12.526	12.821	12.896
0.002	10.559	10.901	10.924	10.886	10.778	10.891	10.922	10.915
0.003	9.748	9.882	9.876	9.841	9.828	9.870	9.875	9.964
0.005	8.691	8.739	8.729	8.705	8.710	8.724	8.722	8.714
0.007	8.069	8.095	8.087	8.070	8.071	8.079	8.076	8.070
0.01	7.498	7.512	7.506	7.495	7.489	7.493	7.491	7.487
0.02	6.655	6.659	6.657	6.653	6.654	6.638	6.654	6.652
0.03	6.332	6.334	6.333	6.331	-	6.310	-	-
0.04	6.186	6.187	6.186	6.185	-	6.161	-	-
0.05	6.118	6.118	6.118	6.118	-	6.091	-	-
0.06	6.086	6.086	6.086	6.086	-	6.059	-	-
0.07	6.072	6.071	6.072	6.072	-	6.043	-	-
0.10	6.066	6.060	6.066	6.060	-	6.031	-	-

TABLE 7.2
|T-T-Wall-Power| and |T-T-Flow-Power| vs. Re and $R_{c,min}$, where $\omega^2 - 6^2 = \omega_{i=2}^2 - 6^2$; cf. equation (6.8).

Re	500-b	1000-b	2000-b	4000-b	700-c	1000-c	1500-c	2000-c
$\omega_{i=2}$	47.970	36.701	30.793	28.013	41.849	36.790	32.792	30.767
$\omega^2 - 6^2$	2265	1311	912	749	1715	1318	1039	911
TTWP	2.265	0.6555	0.228	0.0936	1.225	0.6588	0.3464	0.2277
$R_{\text{c,min}}$		1260				1190		
TTFP	0.7906	0.4905	0.2524	0.1610	0.7824	0.6167	0.4582	0.3660
$R_{\text{c,min}}$		910				1230		

Similarly, for (c) $J_0 = 101$, |T-T-Wall-Power|, Re1$= 1000$, and Re2$= 1500$,

$$\frac{R_{\text{c,min}} - 1000}{0.5429 - 0.6588} = \frac{1500 - 1000}{0.3464 - 0.6588}, \qquad \text{so} \qquad R_{\text{c,min}} = 1190.$$

In the case of |T-T-Wall-Power| in this study, both calculated values of $R_{\text{c,min}}$ are close to the observed experimental values of about 1100–1400 (see Table 1.1). When using |T-T-Flow-Power| in the previous study [10], the calculated value for $J_0 = 51$ is somewhat smaller than the experimental value although the value for $J_0 = 101$ is close to its corresponding experimental value. The approximation for the pressure field needs to be reconsidered in future investigations.

In summary, it is clear that |T-T-Wall-Power| and |T-T-Flow-Power| vs. ΔKE flux are possible methods for calculating R_{c}.

8. Discussion. We consider the wall vorticity vs. the transverse mesh size Δy, (3.11).

The wall surface is $(y = h)$, and the center of vorticity on the wall is $(y = h - (1/2)\Delta y)$ so that the center of vorticity is approximated as $(y = h)$, as displayed in Figure 3.3, where

ETNA
Kent State University and
Johann Radon Institute (RICAM)

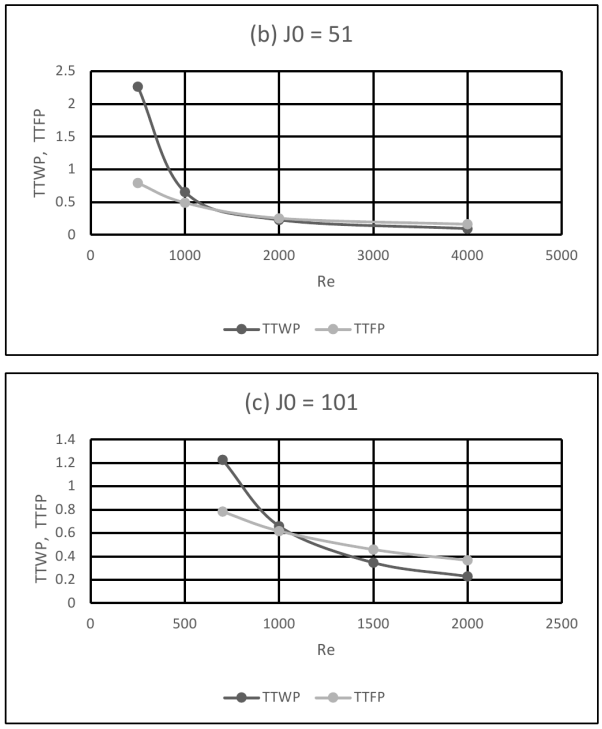

FIG. 7.1. *|T-T-Wall-Power| and |T-T-Flow-Power| for the mesh systems (b) $J_0 = 51$ and (c) $J_0 = 101$.*

the numbers 1–5 indicate the velocities $u(1)$–$u(5)$, respectively;

$$\begin{aligned}
u(1) &= 0,\\
u(2) &= \frac{C}{h^2}[h^2-(h-\Delta y)^2] = \frac{C}{h^2}[2h\Delta y-(\Delta y)^2],\\
u(3) &= \frac{C}{h^2}[h^2-(h-2\Delta y)^2] = \frac{C}{h^2}[4h\Delta y-4(\Delta y)^2],\\
&\vdots\\
u(5) &= \frac{C}{h^2}[h^2-(h-4\Delta y)^2] = \frac{C}{h^2}[8h\Delta y-16(\Delta y)^2].
\end{aligned}$$

The vorticity on the wall is calculated from (7.5):

(b) the mesh size is $(2\Delta y)$ and uses $u(1), u(3), u(5)$;

(c) the mesh size is Δy and uses $u(1), u(2), u(3)$.

Then,

$$\omega(b) = \left(4\frac{C}{h^2}[4h\Delta y-4(\Delta y)^2]-\frac{C}{h^2}[8h\Delta y-16(\Delta y)^2]\right)\frac{1}{2(2\Delta y)} = \frac{2C}{h}$$

and

$$\omega(c) = \left(4\frac{C}{h^2}[2h\Delta y-(\Delta y)^2]-\frac{C}{h^2}[4h\Delta y-4(\Delta y)^2]\right)\frac{1}{2(\Delta y)} = \frac{2C}{h}.$$

ETNA
Kent State University and
Johann Radon Institute (RICAM)

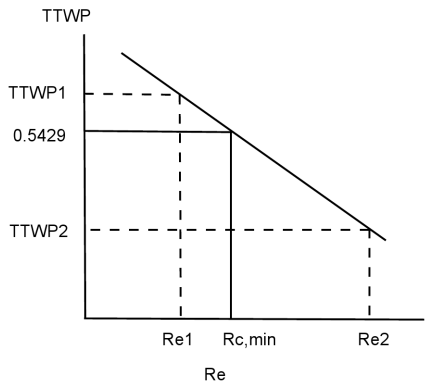

FIG. 7.2. *Linear interpolation for |T-T-Wall-Power| and $R_{c,min}$.*

Thus, if the velocity distribution near the wall is quadratic, then $\omega(b) = \omega(c)$ under different transverse mesh sizes. The calculated results for the vorticity on the wall is nearly the same for (b) $J_0 = 51$ and (c) $J_0 = 101$ at Re $= 1000$ as can be seen in Table 7.1.

9. Conclusions. L-to-T transition occurs only in the entrance region under natural disturbance conditions, and the transition point is near the pipe or channel inlet, not the inlet.

In this paper we have studied ΔKE flux by the introduction of T-Wall-Power, which arises due to the transverse component of the viscous term (T-Wall-Force) in the Navier-Stokes equations on the wall. Accordingly, the hypothesized criterion for laminar-turbulent transition can be tersely expressed as follows: L-T transition occurs if and only if |T-T-Wall-Power| $< \Delta$KE flux. The criterion simply implies that if a channel flow develops into Poiseuille flow, then transition does not occur, and if not, then transition occurs.

T-Wall-Power clarified that under natural disturbance conditions:

(1) T-Wall-Power and ΔKE flux are effective only in the entrance region so that in determining R_c, T-Wall-Force is a possible primary cause of the transition process;

(2) the Reynolds number becomes a critical Reynolds number, i.e., Re = R_c, when |T-T-Wall-Power| = ΔKE flux;

(3) the R_c value depends greatly upon the roundness of the entrance or depth-contraction ratio and upon the flow conditions at the inlet. Thus R_c has minimum values of $R_{c,min} = 1260$ for (b) $J_0 = 51$ and 1190 for (c) $J_0 = 101$, when using a sharp-edged entrance channel;

(4) therefore, the assumptions outlined in Section 1.3 have been confirmed, and

(5) we have devised the wall control-volume method, i.e., by the method, it is clear that A-Wall-Force is the primary cause for the axial pressure drop and T-Wall-Force is that for the transverse pressure drop or ΔKE flux, resulting in equation (2.3).

Acknowledgments. The author wishes to express his sincere appreciation to Professors M. Cohen and M. Honma of the University of Aizu and to Professor Emeritus F. Stenger of the University of Utah for long-term encouragement and valuable technical advice. The author thanks S. Kindermann for his helpful advice as managing editor of ETNA.

ETNA
Kent State University and
Johann Radon Institute (RICAM)

Appendix A. Notation.

b	=	channel width
D	=	pipe diameter
f	=	Darcy-Weisbach friction factor (2.3)
h	=	one-half of the channel height
H	=	channel height or depth (= $2h$),
	=	enthalpy (3.1)
i	=	axial point of mesh system
I_0	=	maximum number of axial mesh points
j	=	transverse point of mesh system
J_0	=	maximum number of transverse mesh points
K	=	minor pressure loss (2.2)
L_e	=	dimensionless entrance length ($x_e/(H\mathrm{Re})$)
p	=	pressure
$\mathcal{P}$	=	pressure ($\mathcal{P} = -p$, (2.3))
Q	=	volumetric flux (bHV_m)
R_c	=	critical Re for L-T transition
R_c1	=	R_c under small disturbance conditions
R_c2	=	R_c under medium disturbance conditions
R_c3	=	R_c under reverse transition conditions
$R_\mathrm{c,min}$	=	minimum R_c
Re	=	Reynolds number for channel flow (HV_m/ν),
	=	Reynolds number for pipe flow (DV_m/ν)
R_t	=	transition Reynolds number, $R_\mathrm{c} < R_t$
Rx	=	length Reynolds number for boundary-layer flow (xV_m/ν)
u, v, w	=	Cartesian velocity components
U_{int}	=	internal energy of a fluid
V	=	velocity vector (u, v, w)
V_m	=	mean velocity in channel flow
$\mathcal{V}$	=	flow region volume
x, y, z	=	Cartesian coordinates
x'	=	dimensionless x-coordinate (x/H)
x_e	=	entrance length from inlet
x_t	=	transition length from inlet
X	=	dimensionless X-coordinate for channel flow ($x/(H\mathrm{Re})$)
X_t	=	dimensionless transition length ($x_t/(H\mathrm{Re})$)
y	=	transverse or y coordinate
μ	=	viscosity coefficient
ν	=	kinematic viscosity (μ/ρ)
ρ	=	density
τ_w	=	wall shear stress (4.1)
ω	=	vorticity
ψ	=	stream function
ΔKE flux	=	increase in kinetic energy flux (6.4)
$(\Delta p)_{wc}$	=	transverse pressure drop between the pressures on the wall and the centerline

REFERENCES

[1] M. A. BADRI NARAYANAN AND T. NARAYANA, *Some studies on transition from laminar to turbulent flow in a two-dimensional channel*, Z. Angew. Math. Mech., 18 (1967), pp. 642–650.

ETNA
Kent State University and
Johann Radon Institute (RICAM)

[2] M. A. BADRI NARAYANAN, *An experimental study of reverse transition in two-dimensional channel flow*, J. Fluid Mech., 31 (1968), pp. 609–623.
[3] R.-Y. CHEN, *Flow in the entrance region at low Reynolds numbers*, J. Fluids Eng., 95 (1973), pp. 153–158.
[4] D. R. CARLSON, S. E. WIDNALL, AND M. F. PEETERS, *A flow-visualization study of transition in plane Poiseuille flow*, J. Fluid Mech., 121 (1982), pp. 487–505.
[5] S. J. DAVIES AND C. M. WHITE, *An experimental study of the flow of water in pipes of rectangular section*, Proc. Royal Soc. A, 119 (1928), pp. 92–107.
[6] S. GOLDSTEIN, *Modern Developments in Fluid Dynamics Vol. I*, Dover, New York, 1965.
[7] R. A. GRANGER, *Fluid Mechanics*, Dover, New York, 1995.
[8] J. P. HARTNETT, J. C. Y. KOH, AND S. T. MCCOMAS, *A comparison of predicted and measured friction factors for turbulent flow through rectangular ducts*, J. Heat Transfer, 84 (1962), pp. 82–88.
[9] H. KANDA, *Computerized model of transition in circular pipe flows. Part 2. Calculation of the minimum critical Reynolds number*, in Proc. ASME Fluids Engeneering Division-1999, D. E. Stock, ed., ASME FED-Vol. 250, ASME, New York, 1999, pp. 197–204.
[10] ———, *Laminar-turbulent transition: Calculation of minimum critical Reynolds number in channel flow,* in Kyoto Conference on the Navier-Stokes Equations and their Applications, Y. Giga, H. Kozono, H. Okamoto, and Y. Shibata, eds., RIMS Kokyuroku Bessatsu B1, RIMS, Kyoto, 2007, pp. 199–217.
[11] ———, *Transition to turbulence in pipe flow: Experimental conditions for minimum critical Reynolds number*, JSFM Proc. Annual Meeting, JSFM, 2013, 27.pdf.
[12] ———, *Laminar-turbulent transition in pipe flow: Wall effects and critical Reynolds number*, Electron. Trans. Numer. Anal., 44 (2015), pp. 548–571.
http://etna.math.kent.edu/vol.44.2015/pp548-571.dir/pp548-571.pdf
[13] H. KANDA AND T. YANAGIYA, *Hysteresis curve in reproduction of Reynolds' color-band experiments*, J. Fluids Engrg., 130 (2008), Art. 051202, 10 pages.
[14] M. A. KARNITZ, M. C. POTTER, AND M. C. SMITH, *An experimental investigation of transition of a plane Poiseuille flow*, J. Fluids Eng., 96 (1974), pp. 384–388.
[15] D. KONDEPUDI AND I. PRIGOGINE, *Modern Thermodynamics*, Wiley, Chichester, 1998.
[16] R. J. LEITE, *An experimental investigation of the stability of Poiseuille flow*, J. Fluid Mech., 5 (1959), pp. 81–96.
[17] G. LEMOULT, J.-L. AIDER, AND J. E. WESFREID, *Experimental scaling law for the subcritical transition to turbulence in plane Poiseuille flow*, Phys. Rev. E, 85 (2012), Art. 025303(R), 5 pages.
[18] E. R. LINDGREN, *The transition process and other phenomena in viscous flow*, Ark. Fys. 12 (1957), pp. 1–169.
[19] M. NISHIOKA, S. IIDA, AND Y. ICHIKAWA, *An experimental investigation of the stability of plane Poiseuille flow*, J. Fluid Mech., 72 (1975), pp. 731–751.
[20] R. L. PANTON, *Incompressible Flow*, Wiley, New York, 1984.
[21] V. C. PATEL AND M. R. HEAD, *Some observations on skin friction and velocity profiles in fully developed pipe and channel flows*, J. Fluid Mech., 38 (1969), pp. 181–201.
[22] O. REYNOLDS, *An experimental investigation of the circumstances which determine whether the motion of water shall be direct or sinuous, and of the Law of resistance in parallel channels*, Philos. Trans. Royal Soc. London, 174 (1883), pp. 935–982.
[23] M. A. RIVAS, JR., AND A. H. SHAPIRO, *On the theory of discharge coefficients for rounded-entrance flowmeters and venturis*, Trans. ASME, 78 (1956), pp. 489–497.
[24] P. J. ROACHE, *Fundamentals of Computational Fluid Dynamics*, Hermosa, Albuquerque, 1998.
[25] M. SANO AND K. TAMAI, *A universal transition to turbulence in channel flow*, Nature Phys., 12 (2016), pp. 249–253.
[26] D. SEKI AND M. MATSUBARA, *Experimental investigation of relaminarizing and transitional channel flows*, Phys. Fluids, 24 (2012), Art. 124102, 23 pages.
[27] R. K. SHAH AND A. L. LONDON, *Advances in Heat Transfer*, Academic Press, New York, 1978.
[28] H. SCHLICHTING, *Boundary-Layer Theory*, McGraw-Hill, New York, 1979.
[29] S. TANEDA, *Gazou-kara Manabu Ryutai Rikigaku* (in Japanese) *(Fluid Dynamics Studied from Image)*, Asakura Shoten, Tokyo, 1993.
[30] G. A. WHAN AND R. R. ROTHFUS, *Characteristics of transition flow between parallel plates*, AIChE Journal, 5 (1959), pp. 204–208.
[31] F. M. WHITE, *Viscous Fluid Flow*, McGraw-Hill, New York, 1991.
[32] ———, *Fluid Mechanics*, McGraw-Hill, New York, 1999.